

## **An Efficient and Accurate Approach for Analysis and Design of High Lift Configurations**

by

Tuncer Cebeci  
MDC Distinguished Fellow  
McDonnell Douglas Corporation

and

Eric Besnard  
Aerospace Engineering Department  
California State University, Long Beach

### **Résumé**

Une méthode de calcul des propriétés aérodynamiques de profils et ailes hypersustentateurs est décrite. La méthode est basée sur un couplage visqueux/non-visqueux utilisant une version améliorée du modèle à viscosité turbulente effective de Cebeci et Smith. Des résultats sont d'abord présentés pour des profils à nombres de Reynolds faibles et modérés. L'importance du calcul de la position de la transition dans le but de déterminer la traînée est mise en évidence. Les résultats montrent également que la version améliorée du modèle Cebeci-Smith permet de calculer des écoulements avec décollements massifs et, par conséquent, de prédire le décrochage. Des résultats (coefficients de pression, de portance, de traînée et de moment de tangage) sont présentés pour une série de profils hypersustentateurs avec bords de fuite et volets déployés. Ensuite, des résultats sont exposés et comparés aux mesures expérimentales pour des ailes avec et sans systèmes hypersustentateurs. L'importance des effets de compressibilité, du rôle joué par le modèle de turbulence au décrochage et, encore une fois, du calcul de transition, est démontrée.

### **Abstract**

A calculation method for the aerodynamic prediction of multi-element airfoils and wings based on an interactive boundary-layer approach using an improved Cebeci-Smith eddy viscosity formulation is described. Results are first presented for single airfoils at low and moderate Reynolds numbers in order to demonstrate the need to calculate transition for accurate drag polar prediction and the ability of the improved Cebeci-Smith turbulence model to predict flows with extensive separation, and therefore to predict maximum lift coefficient. Results, in terms of pressure distributions and lift, drag and moment coefficients, are presented for a series of multi-element airfoils with flaps and slats. Results are then presented for single- and multi-element wing configurations. The importance of the compressibility effects and the turbulence model on stall, and, again, the need to calculate the onset of transition, are demonstrated.

### **Introduction**

In the last thirty years, there have been significant accomplishments in computational fluid dynamics (CFD). Whereas in the early 1960's panel methods and boundary-layer methods were being developed for relatively simple configurations, today we have Navier-Stokes methods not only for simple configurations but also for complex aircraft configurations. Calculations are being routinely performed with these methods leading to significant savings by reducing wind tunnel testing. Progress has been so impressive that one may even say that CFD has reached its maturity.

An area that still requires further work in CFD is the development of design methods for high lift configurations. The presence of high and low Reynolds number flows on various components of airfoils and significant regions of flow separation near stall conditions, as well as possible merging of shear layers, make the development of such a capability a challenging task. The required generality and accuracy of the method and, equally important, its efficiency as a design tool, introduce additional challenges.

The current development of design algorithm for high lift configurations follows two approaches. One approach is based on the solution of the Navier-Stokes equations with structured and unstructured grids. The second approach is the one based on interactive boundary layer theory and will form the basis for our presentation. This approach involves interaction between inviscid and boundary-layer equations. For low speed flows, the inviscid flow is often computed by a panel method, with or without compressibility corrections, and the viscous flow is computed by a boundary-layer method. This approach, though not as general as the Navier-Stokes approach, provides a good compromise between the efficiency and accuracy required in a design process (Nield, 1995).

Regardless of which approach is used to develop a computational tool for high lift configurations, it is necessary to calculate the onset of transition in order to identify the effect of wind tunnel and flight Reynolds numbers. Individual components of multi-element airfoils at wind tunnel Reynolds numbers have relatively lower Reynolds numbers than the main airfoil. At chord Reynolds numbers less than 500,000, the components can have large separation bubbles, with the onset of transition occurring inside the separation bubble. As a result, the behavior of the flow can be significantly different from the behavior of the main airfoil at higher Reynolds numbers. Furthermore, the transition can influence the drag coefficient. For this reason determining the onset transition is crucial for predicting drag polars, which are of major interest when designing high-lift systems for take-off and climb requirements (Nield, 1995).

In addition to the accuracy requirements imposed on a high-lift method, it is necessary that the method is efficient so that the airfoil performance due to component gap, overhang and deflection variations can easily be predicted rapidly and economically.

The method described here has been developed to address these needs and is described in detail in Cebeci (1998) for steady flows over single and multi-element airfoils, unsteady flows over single airfoils and steady flows over single and multi-element wings. In the next two sections we present a brief description of this method for two- and three-dimensional flows, respectively, and in the following two sections we discuss its application to a variety of single and multi-element airfoils and wings. The paper ends with a summary of the more important conclusions.

### **Calculation Method: Two-dimensional Flows**

The calculation method for two-dimensional flows is formulated for compressible flows and has been applied to single and multi-element airfoils at low and high Reynolds numbers. For single airfoils both panel and full potential methods are used to compute the inviscid flow with viscous effects provided by the boundary-layer method. For multi-element airfoils, the inviscid flow is computed by a panel method employing three options with and without compressibility corrections. In one option the vorticity strength was taken to be constant on all panels, and a single value was adjusted to satisfy the condition associated with the specification of circulation. This option is used for all conventional airfoils and is found to be satisfactory. For airfoils with thin trailing edges and/or supercritical airfoils two other options were used. One option assumes that vorticity varies quadratically with the surface distance and the second option assumes that it varies quadratically in a small region near the trailing edge.

The boundary-layer method is based on the solution of the continuity, momentum and energy equations; with the eddy viscosity  $\epsilon_m$  and turbulent Prandtl number  $Pr_t$

concepts, these equations and their boundary condition on the airfoil and in the wake for an adiabatic surface are (Cebeci, 1998):

$$\frac{\partial}{\partial x}(\rho u) + \frac{\partial}{\partial y}(\overline{\rho v}) = 0 \quad (1)$$

$$\rho u \frac{\partial u}{\partial x} + \overline{\rho v} \frac{\partial u}{\partial y} = \rho_e u_e \frac{du_e}{dx} + \frac{\partial}{\partial y} \left( (\mu + \rho \epsilon_m) \frac{\partial u}{\partial y} \right) \quad (2)$$

$$\rho u \frac{\partial H}{\partial x} + \overline{\rho v} \frac{\partial H}{\partial y} = \frac{\partial}{\partial y} \left( (k + c_p \rho \frac{\epsilon_m}{Pr_t}) \frac{\partial T}{\partial y} + u(\mu + \rho \epsilon_m) \frac{\partial u}{\partial y} \right) \quad (3)$$

On the airfoil, the boundary conditions are

$$y = 0, \quad u = 0, \quad v = 0, \quad \frac{\partial H}{\partial y} = 0 \quad (4a)$$

$$y \rightarrow \infty, \quad u \rightarrow u_e(x), \quad H \rightarrow H_e \quad (4b)$$

In the wake, the boundary conditions are written on a dividing line  $y = 0$  which separates the lower and upper portions of the wake

$$y = 0, \quad \frac{\partial u}{\partial y} = 0, \quad v = 0, \quad \frac{\partial H}{\partial y} = 0 \quad (5a)$$

$$y \rightarrow \infty, \quad u \rightarrow u_e(x), \quad H \rightarrow H_e \quad (5b)$$

### Turbulence Model

The turbulence model for  $\epsilon_m$  and  $Pr_t$  is given by an improved version of the Cebeci and Smith algebraic eddy viscosity formulation (Cebeci and Chang, 1996). According to this model,  $Pr_t$  is taken as constant equal to 0.9 and  $\epsilon_m$  is given by separate expressions for the inner and outer regions of the boundary layer,

$$\epsilon_m = \begin{cases} (\epsilon_m)_i = \left( 0.4 y \left( 1 - \exp \frac{-y}{A} \right) \right)^2 \left| \frac{\partial u}{\partial y} \right| \gamma_{tr} & 0 \leq y \leq y_c \\ (\epsilon_m)_o = \alpha \int_0^\infty (u_e - u) dy \left| \gamma_{tr} \gamma \right. & y_c \leq y \leq \delta \end{cases} \quad (6)$$

where

$$\alpha = \frac{0.0168}{F^{1.5}}, \quad A = 26 \frac{v}{u_\tau} \left( \frac{\rho}{\rho_w} \right)^{1/2}, \quad u_\tau = \left( \frac{\tau}{\rho} \right)_{\max}^{1/2} \quad (7)$$

The parameter  $F$  is related to the ratio of the product of the turbulence energy by normal stresses to that by shear stress evaluated at the location where the shear stress is maximum. As discussed in Cebeci (1998), it is given by

$$F = 1 - \beta \frac{\partial u / \partial x}{\partial u / \partial y} \quad (8)$$

where the parameter  $\beta$  is a function of  $R_t = \tau_w / (-\rho \overline{u'v'})_{\max}$ , which, for  $\tau_w \geq 0$ , is represented by

$$\beta = \begin{cases} \frac{6}{1 + 2R_t(2 - R_t)} & R_t \leq 1.0 \\ \frac{1 + R_t}{R_t} & R_t \geq 1.0 \end{cases} \quad (9)$$

For  $\tau_w \leq 0$ ,  $R_t$  is set equal to zero.

Also, whereas in the original Cebeci-Smith eddy viscosity formulation (Cebeci and Smith, 1974) the intermittency expression was valid only for zero pressure gradient flows, in the improved formulation, the intermittency expression is applicable for flows with favorable and adverse pressure gradients as well as zero pressure gradient flows. It is based on Fiedler and Head's correlation and is given by

$$\gamma = \frac{1}{2} \left[ 1 - \operatorname{erf} \left( \frac{y - Y}{\sqrt{2}\sigma} \right) \right] \quad (10)$$

where  $Y$  and  $\sigma$  are general intermittency parameters with  $Y$  denoting the value of  $y$  where  $\gamma = 0.5$  and  $\sigma$  denoting the standard deviation. For details, see Cebeci (1998).

The condition used to define  $y_c$  in Eq. (6) is the continuity of the eddy viscosity, so that  $\varepsilon_m$  is defined by  $(\varepsilon_m)_i$  from the wall outward (inner region) until its value is equal to that given for the outer region by  $(\varepsilon_m)_o$ .

The expression  $\gamma_{tr}$  models the transition region and is given by

$$\gamma_{tr} = 1 - \exp \left( -G(x - x_{tr}) \int_{x_{tr}}^x \frac{dx}{u_e} \right) \quad (11)$$

Here  $x_{tr}$  denotes the onset of transition and  $G$  is defined by

$$G = \frac{3}{C^2} \frac{u_e^3}{\nu^2} R_{x_{tr}}^{-1.34} \quad (12)$$

where  $C$  is 60 for attached flows and  $R_{x_{tr}} = (u_e x / \nu)_{tr}$  is the transition Reynolds number. In the low Reynolds number range from  $R_c = 2 \times 10^9$  to  $6 \times 10^5$ , the parameter  $C$  is given by

$$C^2 = 213 \left( \log R_{x_{tr}} - 4.7323 \right) \quad (13)$$

The corresponding expressions for the eddy-viscosity formulation in the wake are

$$\varepsilon_m = (\varepsilon_m)_w + [(\varepsilon_m)_{t.e.} - (\varepsilon_m)_w] \exp \frac{-(x - x_0)}{\ell_w \delta_{t.e.}} \quad (14)$$

where  $\delta_{t.e.}$  is the boundary layer thickness at the trailing edge,  $\ell_w = 20$ ,  $(\varepsilon_m)_{t.e.}$  is the eddy viscosity at the trailing edge, and  $(\varepsilon_m)_w$  is the eddy-viscosity in the far wake given by the larger of

$$(\varepsilon_m)_w^l = 0.064 \int_{-\infty}^{y_{\min}} (u_e - u) \cdot dy \quad (15a)$$

and

$$(\varepsilon_m)_w^u = 0.064 \int_{y_{\min}}^{\infty} (u_e - u) \cdot dy \quad (15b)$$

with  $y_{\min}$  denoting the location where the velocity is minimum.

#### Interaction Law

To avoid the breakdown of the boundary-layer equations at separation, the above equations, with the turbulence model for  $\varepsilon_m$  and  $Pr_t$ , are solved in the inverse mode by using the interaction law given by Veldman and fully discussed in Cebeci (1998). According to this law, in the interaction region ( $x_a, x_b$ ), the external velocity  $u_e(x)$  is written as

$$u_e(x) = u_e^o(x) + \frac{1}{\pi} \int_{x_a}^{x_b} \frac{d}{d\sigma} (u_e \delta^*) \frac{d\sigma}{x - \sigma} \quad (16)$$

In the inverse mode, with  $u_e''(x)$  corresponding to the inviscid velocity,  $u_e(x)$  is treated as an unknown and is obtained as part of the solution.

*Solution Procedure*

A two-point finite difference method is used to solve the boundary-layer equations as described in Cebeci (1998). Once a solution is obtained for the external velocity distribution given by the panel method, the blowing velocity distribution on the surface is calculated from

$$v_b = \frac{d}{dx} (u_e \delta^*) \tag{17}$$

and a jump  $\Delta v_b$  in the component of velocity normal to the airfoil dividing streamline

$$\Delta v_b = \frac{d}{dx} (u_e^u \delta_u^*) + \frac{d}{dx} (u_e^\ell \delta_\ell^*) \tag{18}$$

is computed from the boundary-layer solutions. In the above equation subscripts and superscripts  $u$  and  $\ell$  denote upper and lower sides of the dividing streamline. The boundary conditions given by Eqs. (17) and (18) are then used in the panel method to replace the zero blowing velocity at the surface, and the calculated displacement thickness at the airfoil trailing edge is used to satisfy the Kutta condition. This procedure (Figure 1) of computing inviscid and viscous flows is continued until the convergence of the solutions, as described in Cebeci (1998).

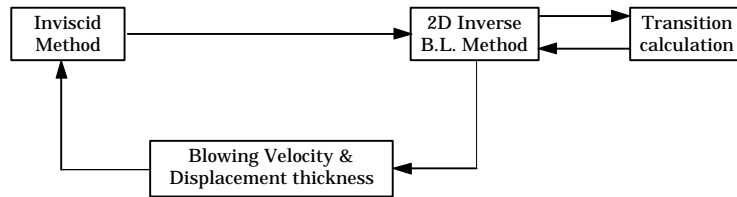


Figure 1. Calculation method for two-dimensional flows.

**Calculation Method: Three-dimensional Flows**

In principle the calculation method for three-dimensional flows is similar to that described for two-dimensional flows. Its ingredients are shown in Figure 2. The purpose of the interface program placed between the inviscid and three-dimensional inverse boundary-layer methods is to process the geometry and inviscid velocity data for input to the boundary-layer program. The basic input to this program is the definition of the wing configuration, which is used by a geometry subroutine to construct a nonorthogonal coordinate system and compute the associated geometrical parameters consisting of geodesic curvatures and metric coefficients needed in the boundary-layer calculations. Some of the generated data are used to transform the inviscid velocity components on the surface calculated in a Cartesian coordinate system into the boundary-layer coordinate system. This operation consists of dot products of velocity vectors as well as chordwise and spanwise interpolation. Further velocity and geometry data processing is done in a subroutine which separates the generated information into upper and lower surfaces of the wing for boundary-layer calculations. For further details, see Cebeci (1998).

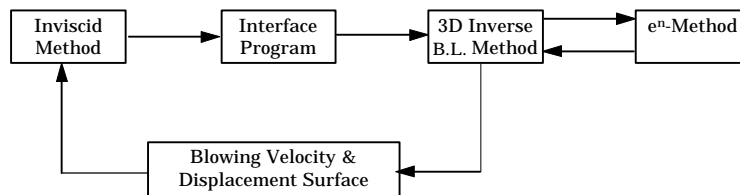


Figure 2. The calculation method for three-dimensional flows.

The inviscid flow is computed by the Hess surface-source panel method applicable to a complete airplane configuration. In this method a general body is represented by means of a set of quadrilateral panels, as shown in Figure 3. In general, a three-dimensional configuration consists of lifting sections, such as a wing or pylon for which there is a well-defined trailing edge, and nonlifting sections, such as fuselage. Under the Hess formulation, all panels are assigned an independent source distribution, while those on a lifting section are also assumed to carry a bound vorticity distribution. The variation of this bound vorticity in the streamwise direction is assumed, while its variation in the spanwise direction is adjusted to satisfy the Kutta condition at the trailing edge. The complete solution for a prescribed flow condition is, therefore, obtained by simultaneously satisfying a condition of zero normal velocity at a control point on each panel of the body together with a Kutta condition at each trailing edge panel.

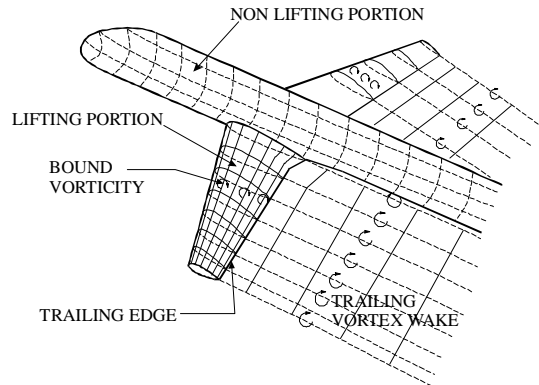


Figure 3. Wing/body configuration

The boundary-layer method is based on the solution of the boundary-layer equations expressed in a nonorthogonal coordinate system. For a body-fitted coordinate system, these equations, with the eddy viscosity concept, are

Continuity Equation

$$\frac{\partial}{\partial x}(uh_2 \sin\theta) + \frac{\partial}{\partial z}(wh_1 \sin\theta) + \frac{\partial}{\partial y}(vh_1h_2 \sin\theta) = 0 \quad (19)$$

x-Momentum Equation

$$\begin{aligned} \frac{u}{h_1} \frac{\partial u}{\partial x} + \frac{w}{h_2} \frac{\partial u}{\partial z} + v \frac{\partial u}{\partial y} - k_1 u^2 \cot\theta + k_2 w^2 \operatorname{cosec}\theta + k_{12} uw \\ = - \frac{\operatorname{cosec}^2 \theta}{\rho h_1} \frac{\partial p}{\partial x} + \frac{\cot\theta \operatorname{cosec}\theta}{\rho h_2} \frac{\partial p}{\partial z} + v \frac{\partial}{\partial y} \left( b \frac{\partial w}{\partial y} \right) \end{aligned} \quad (20)$$

z-Momentum Equation

$$\begin{aligned} \frac{u}{h_1} \frac{\partial w}{\partial x} + \frac{w}{h_2} \frac{\partial w}{\partial z} + v \frac{\partial w}{\partial y} - k_2 u^2 \cot\theta + k_1 w^2 \operatorname{cosec}\theta + k_{21} uw \\ = \frac{\cot\theta \operatorname{cosec}\theta}{\rho h_1} \frac{\partial p}{\partial x} - \frac{\operatorname{cosec}^2 \theta}{\rho h_2} \frac{\partial p}{\partial z} + v \frac{\partial}{\partial y} \left( b \frac{\partial w}{\partial y} \right) \end{aligned} \quad (21)$$

Here  $x$  denotes the axial direction,  $z$  the spanwise direction, and  $y$  is normal to the surface. Also  $h$  denotes the metric coefficients,  $k$  the curvature parameters,  $\theta$  the angle between the coordinate lines  $x = \text{const.}$  and  $z = \text{const.}$ , and  $b$  contains the turbulent terms.

The above equations, together with those for the plane of symmetry and along the chordwise direction, are solved by two-point finite-difference method described in Cebeci (1998), subject to the following boundary conditions:

$$y = 0, \quad u = 0, \quad v = 0, \quad w = 0 \quad (22a)$$

$$y = \delta, \quad u = u_e(x, z), \quad w = w_e(x, z) \quad (22b)$$

Again to account for flow separation, the equations are solved in an inverse mode. Veldman's interaction law was modified to account for the interaction in the  $x$ - and  $z$ -directions in three steps. In step one, an initial displacement surface is generated by solving a quasi-three-dimensional form of Eqs. (19) to (21) with all derivatives with respect to  $z$  neglected, that is

$$\frac{\partial}{\partial x}(uh_2 \sin\theta) + \frac{\partial}{\partial y}(vh_1h_2 \sin\theta) = 0 \quad (23)$$

$$\frac{u}{h_1} \frac{\partial u}{\partial x} + v \frac{\partial u}{\partial y} - k_1 u^2 \cot\theta + k_2 w^2 \operatorname{cosec}\theta + k_1 uw = -\frac{\operatorname{cosec}^2 \theta}{\rho h_1} \frac{\partial p}{\partial x} + v \frac{\partial}{\partial y} \left( b \frac{\partial u}{\partial y} \right) \quad (24)$$

$$\frac{u}{h_1} \frac{\partial w}{\partial x} + v \frac{\partial w}{\partial y} - k_2 w^2 \cot\theta + k_1 u^2 \operatorname{cosec}\theta + k_{21} uw = \frac{\cot\theta \operatorname{cosec}\theta}{\rho h_1} \frac{\partial p}{\partial z} + v \frac{\partial}{\partial y} \left( b \frac{\partial w}{\partial y} \right) \quad (25)$$

with the external velocity distribution  $u_e^o(x)$  obtained from the panel method. The second step involves interaction between the inviscid flow equations and the quasi-three-dimensional flow equations. As in two-dimensional flows, the solutions of the boundary-layer equations are used to compute distributions of blowing velocity on the surface, and these allow updating the inviscid flow solutions. In step three, after the calculation of the initial conditions in the  $(y, z)$  and  $(x, y)$  planes, the fully three-dimensional boundary-layer equations are solved with the external velocity components resulting from step two. As before, the spanwise velocity component is assumed to correspond to its inviscid value. The viscous flow solutions are obtained by marching in the spanwise direction at each advancing chordwise location. This represents the first phase in an interactive loop that involves the fully three-dimensional boundary-layer equations. In the subsequent phases, as before, the blowing velocity distribution is used to obtain improved inviscid flow solutions so that the fully three-dimensional boundary-layer equations can be solved in accordance with the iteration scheme shown in Figure 2. For further details, including the eddy viscosity formulation for three-dimensional flows, see Cebeci (1998).

The onset of transition locations needed in the boundary-layer method are calculated by using the  $e^n$ -method with the Cebeci-Stewartson eigenvalue formulation as described in Cebeci (1998). Its calculation, while important for airfoils, is of utmost importance for three-dimensional flows. Unlike two-dimensional flows where transition occurs in the region where the flow decelerates, in three-dimensional flows it can occur in the region where the flow accelerates. The sweep angle and Reynolds number strongly influence the location of transition and require that the calculation of transition becomes part of the computational strategy.

In the calculation method for three-dimensional flows, the stability/transition calculations are first performed for three-dimensional laminar boundary layers obtained for a prescribed pressure distribution, so that the inviscid and viscous flow equations can then be solved according to the interaction scheme shown in Figure 2. The quasi-three-dimensional forms of the equations are solved chordwise in the inverse mode to obtain the interaction coefficients needed in the solution of the full three-dimensional boundary-layer equations. Several sweeps on the wing and in the wake are performed, and new inviscid flow solutions with viscous effects are obtained. The procedure is repeated until the solutions converge; the transition calculations are then repeated to obtain new transition

locations on the wing for the next phase of the interactive boundary-layer calculations. The whole process is repeated until the flowfield and transition locations converge.

### Results and Discussion: Two-dimensional Flows

Before presenting results for multi-element airfoils and wings, it is useful to analyze results for single airfoils at low and high Reynolds numbers, and for incompressible and low Mach number flows.

#### Single Airfoils

##### Airfoils at High Reynolds Numbers

Figure 4 presents a comparison between measured (Abbott *et al.*, 1959) and computed lift and drag coefficients for the NACA 0012 airfoil at a chord Reynolds number of  $3 \times 10^6$ . To demonstrate the importance of computing transition as part of the method, calculations were also performed with transition fixed near the stagnation point for all angles of attack (dotted line in Figure 4). As can be seen, results with computed transition show a much better agreement with experimental data than those in which the transition was fixed.

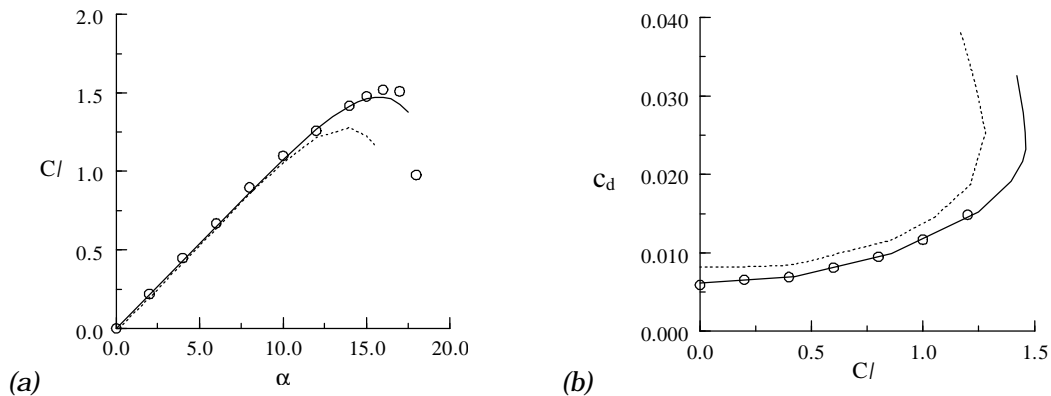


Figure 4. Comparison of measured (symbols) and calculated (lines) (a) lift and (b) drag coefficients for the NACA 0012 airfoil at  $R_c = 3 \times 10^6$ . Continuous lines denote calculations with computed transition, and dotted lines results with transition near the stagnation point.

##### Airfoils at Low Reynolds Numbers

The behavior of airfoils at low Reynolds numbers differs from that at high Reynolds numbers, in that rather large separation bubbles can occur downstream of the leading edge with transition taking place within the bubble prior to reattachment. The length of the bubble increases with decreasing Reynolds numbers and strongly influences the performance characteristics of the airfoil. At low to moderate angles of attack, the onset of transition is calculated with the  $e^n$ -method. At higher angles of attack, it is not possible to calculate the onset of transition with the  $e^n$ -method. For this reason, the onset of transition is assumed to correspond to the location of laminar flow separation.

Results are first presented for the ONERA-D airfoil tested by Cousteix and Pailhas (1979) in a wind tunnel with a chord Reynolds number of  $3 \times 10^5$  at zero angle of attack. The airfoil and mean velocity profiles and distributions of external velocity and skin-friction coefficient are shown in Figure 5. Measured and calculated results are in close agreement with appreciable differences only in the velocity profiles immediately upstream of boundary-layer separation where we may expect cross-stream pressure gradients and normal stresses to have a locally-important role. In this case, transition occurred within the separated flow region and caused reattachment shortly thereafter. The calculations revealed transition at

$x/c = 0.79$  for  $n = 8$ , at  $x/c = 0.81$  for  $n = 9$  in the  $e^n$ -method, in comparison with measurements which revealed transition at  $x/c = 0.808$ .

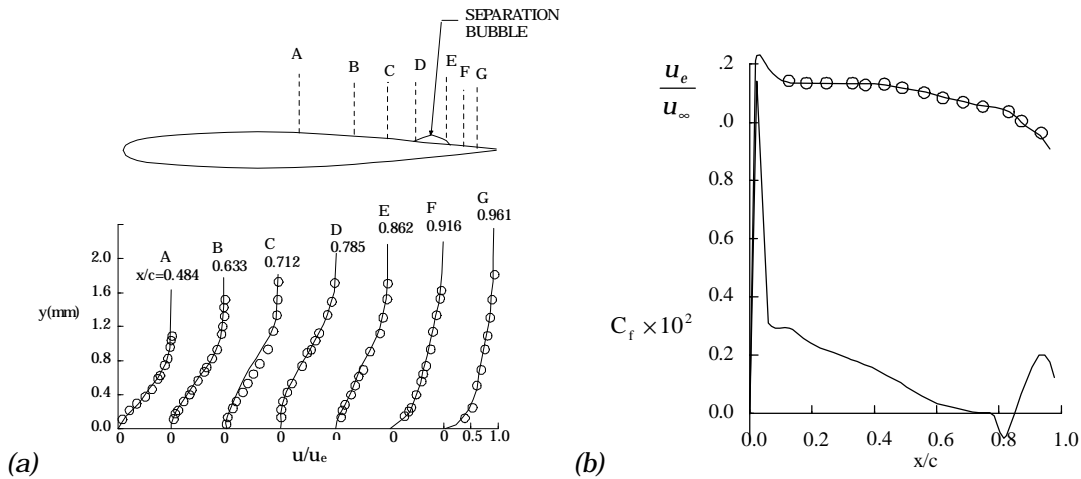


Figure 5. Comparison of calculated (solid lines) and measured (symbols) (a) velocity profiles and (b) external velocity and skin friction coefficient distributions for the upper surface of the ONERA-D airfoil for  $\alpha = 0^\circ$ ,  $R_c = 3 \cdot 10^5$ .

Figure 6 shows the results for the Eppler 387 airfoil at a chord Reynolds number of 200,000. The experimental data for this airfoil was obtained (McGhee *et al.*, 1988) in the Langley Low-Turbulence Pressure Tunnel (LTPT). Agreement is generally good, including at stall.

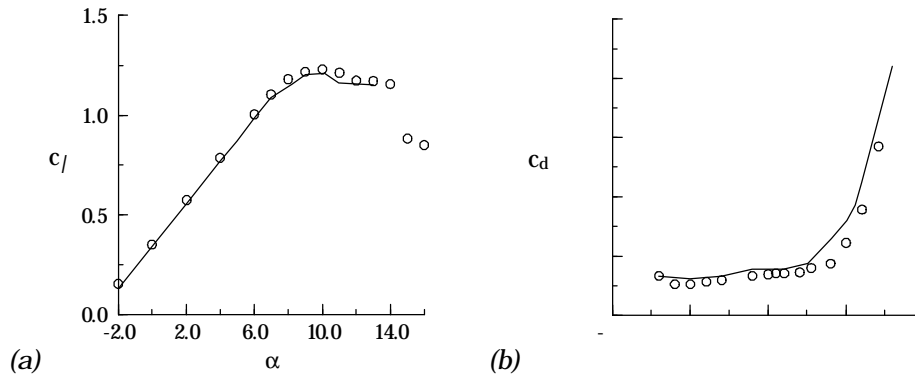


Figure 6. Force coefficients for the Eppler 387 airfoil at  $R_c = 200,000$ , (a) lift and (b) drag. Circles denote experimental data, continuous lines denote calculations with computed transition.

### Airfoils at Low Mach Numbers

Although high lift systems usually operate at low Mach numbers –about  $M_\infty = 0.25$ –, their performance can be affected by compressibility effects. The calculation method is applied here to account for the compressibility effects. Results at  $R_c = 4 \times 10^6$ ,  $M_\infty = 0.30$  are presented in Figure 7a for the NACA 0012 airfoil and Figure 7b for a NASA supercritical airfoil (Omar *et al.*, 1977). Results obtained with the present method are compared with those obtained with a compressible Navier-Stokes method (Cebeci and Chang, 1996) employing the same turbulence model and show that agreement with experimental data is as good, while computer requirements were much lower.

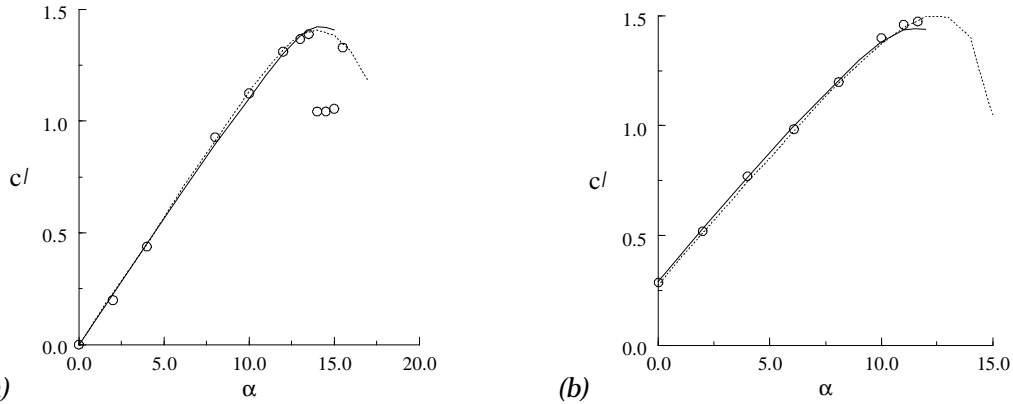


Figure 7. Comparison between measured lift coefficients (circles) and those obtained with the present method (dotted lines) and a compressible Navier-Stokes method for (a) the NACA 0012 airfoil and (b) a NASA supercritical airfoil.

Two-element Airfoils

Figures 8 and 9 show a comparison between measurements (van den Berg and Oskam, 1979) and results for the NLR 7301 supercritical airfoil/flap configuration with a flap of 32% chord deflected at an angle of  $20^\circ$  and with a gap of 2.6% chord. The experimental free stream Mach number was  $M_\infty = 0.185$ , and the chord Reynolds number was  $2.51 \times 10^6$ . Figure 8 shows a comparison between measured and computed pressure distributions at  $\alpha = 6.0^\circ$  and  $\alpha = 13.1^\circ$ , and Figure 9 shows a similar comparison for the lift coefficient and drag polar. Calculated results, including drag, agree well with experimental data.

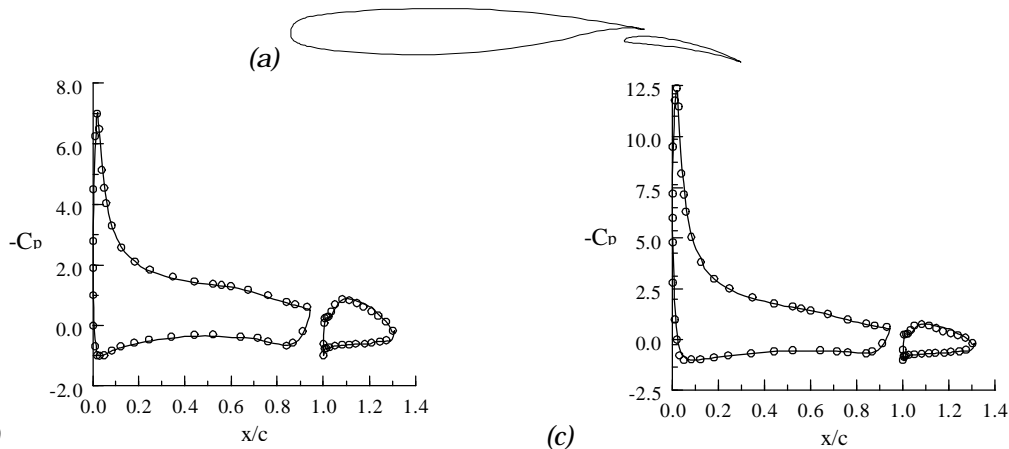


Figure 8. Comparison of measured (symbols) and calculated (continuous lines) pressure distributions for (a) the NLR 7301 supercritical airfoil/flap configuration at (b)  $\alpha = 6^\circ$  and (c)  $\alpha = 13.1^\circ$ .

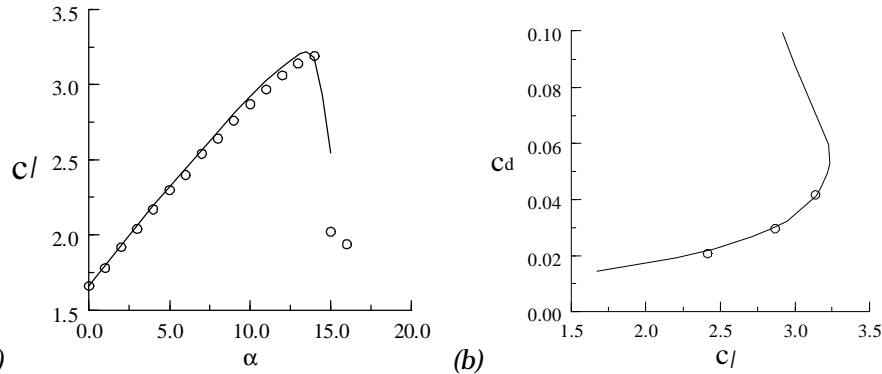


Figure 9. Comparison of measured (symbols) and calculated (continuous lines) (a) lift and (b) drag coefficients for the NLR 7301 supercritical airfoil/flap configuration.

Figures 10 to 12 show a comparison between results and experimental data for a NASA high lift configuration (Omar *et al.*, 1977) for a free stream Mach number of  $M_\infty = 0.201$  and chord Reynolds number of  $2.83 \times 10^6$ . The compressibility corrections to the inviscid flow were made using the Prandtl-Glauert formula.

Figure 10 shows the pressure distributions for an airfoil/flap configuration at  $\alpha = 0.01^\circ$  and  $8.93^\circ$ . It is seen that the calculated results are in good agreement with experimental data, although there is some discrepancy on the upper surface of the flap. This discrepancy is due to two phenomena, the merging of shear layers and the inaccurate wake center line prediction, as shown in Figure 11. It is seen that in the experiments merging occurs at the trailing edge of the flap for both  $\alpha = 0^\circ$  and  $\alpha = 8^\circ$ , and that it is not predicted by the present method. Also, in the present method, the wake center line is assumed to be the dividing streamline originating at the main element trailing edge and is closer to the flap upper surface than the measured one (thick line in Figure 11), which causes a greater predicted flow acceleration on the flap upper surface than the actual acceleration.

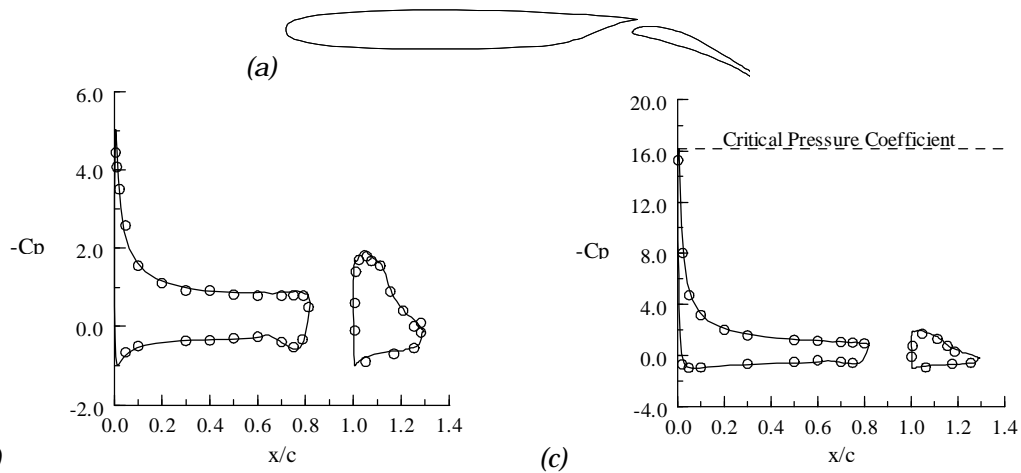


Figure 10. Comparison of measured (symbols) and calculated (continuous lines) pressure distributions for (a) the NASA airfoil/flap configuration at (b)  $\alpha = 0.01^\circ$  and (c)  $\alpha = 8.93^\circ$ .

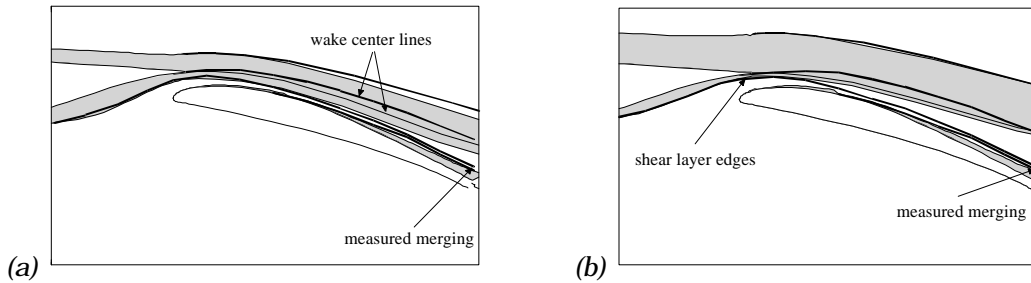


Figure 11. Comparison of measured and computed shear layers for the NASA airfoil/flap configuration, (a)  $\alpha = 0^\circ$  and (b)  $\alpha = 8^\circ$ . Shaded areas denote computed shear layers and thick lines denote edges of measured shear layers.

Figure 12 shows the lift and drag coefficients for the same configuration. The lift coefficient is slightly over predicted due to the discrepancies on the flap upper surface and, similarly, the drag coefficient is slightly under predicted. Also, the calculated incompressible stall angle is rather different from the calculated compressible one. The critical pressure coefficient for  $M_\infty = 0.201$  is indicated in Figure 10c. At  $\alpha = 8.93^\circ$ , the measured stall angle, there exists a small region of supersonic flow and a shock may occur. Even though this shock cannot be predicted by the panel method, the compressibility corrections, theoretically applicable at lower angles of attack only, provide a significant improvement to the stall prediction. However, a truly compressible method such as the one of Verhoff, Chen, and Cebeci (1996) would be preferable.

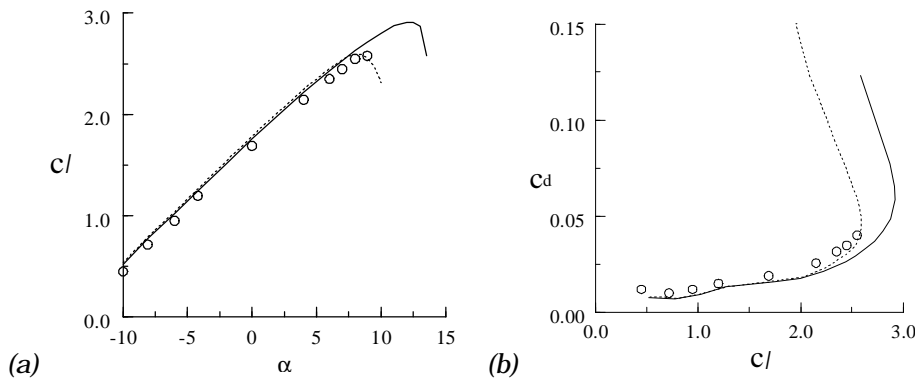


Figure 12. Comparison of measured (symbols) and calculated (lines) (a) lift coefficients, and (b) drag polars for the NASA airfoil/flap configuration. Continuous lines denote incompressible calculations and dotted lines compressible calculations.

#### Slat-airfoil-flap Configurations

The previous section and calculations reported previously (Cebeci, Besnard, and Chen, 1996) demonstrated the ability of the method to compute multi-element airfoil lift and drag coefficients accurately, including stall and post-stall, for slat-airfoil and airfoil-flap configurations. For these cases, stall is mostly due to flow separation occurring on the main element and is well predicted by the present method. For well-optimized slat-airfoil-flap configurations, however, stall often occurs without flow separation on the main element. Instead, the slat wake merges into the main element boundary layer or wake and, due to the adverse pressure gradient induced by the presence of the flap; this complex shear layer may drastically thicken downstream of the main element trailing edge, thus reducing the overall circulation and causing a reduction in lift.

To illustrate this phenomenon and evaluate the ability of the present method to predict such flows, a three-element airfoil (Moir, 1994) was considered for a free stream Mach number of about  $M_\infty = 0.2$  and chord Reynolds number of  $3.52 \times 10^6$ . The slat is deflected at  $25^\circ$  and the

flap at  $20^\circ$ . Figure 13 shows a comparison of the calculated and measured pressure distributions at  $\alpha = 4^\circ$  and  $\alpha = 20^\circ$ . Figure 14 shows a similar comparison for the integrated lift, drag and moment coefficients. Agreement is generally good up to stall. Discrepancies exist in the flap well on the main element and near the leading edge of the flap because current results were obtained by using a fairing of the flap well. Work is in progress to improve the flap well procedure of Cebeci, Besnard, and Chen (1996) in order to refine predictions in this region. It is conjectured that the discrepancies in lift, drag and moment coefficients are partially due to this phenomenon. Also, as previously mentioned, the merging of shear layers was not accounted for and may have contributed to the differences between experimental data and calculations.

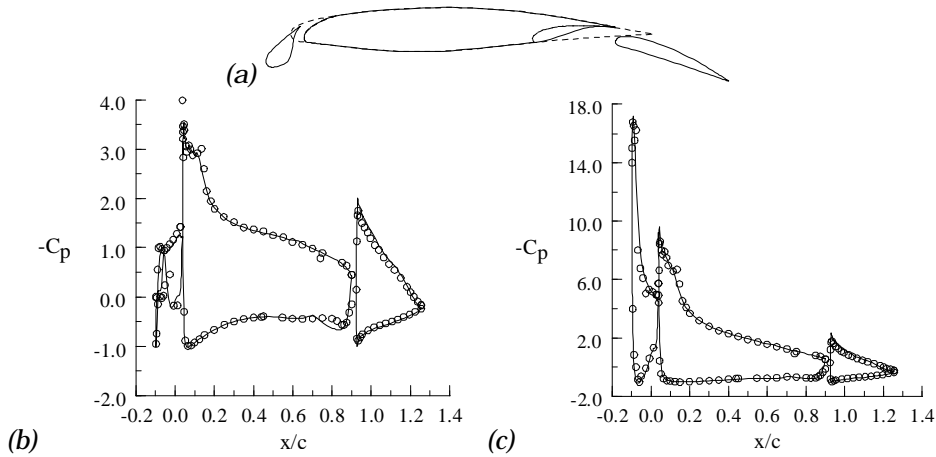


Figure 13. Comparison of calculated (continuous lines) and measured (symbols) pressure distributions for (a) a three-element airfoil at (b)  $\alpha = 4^\circ$  and (c)  $\alpha = 20^\circ$ .

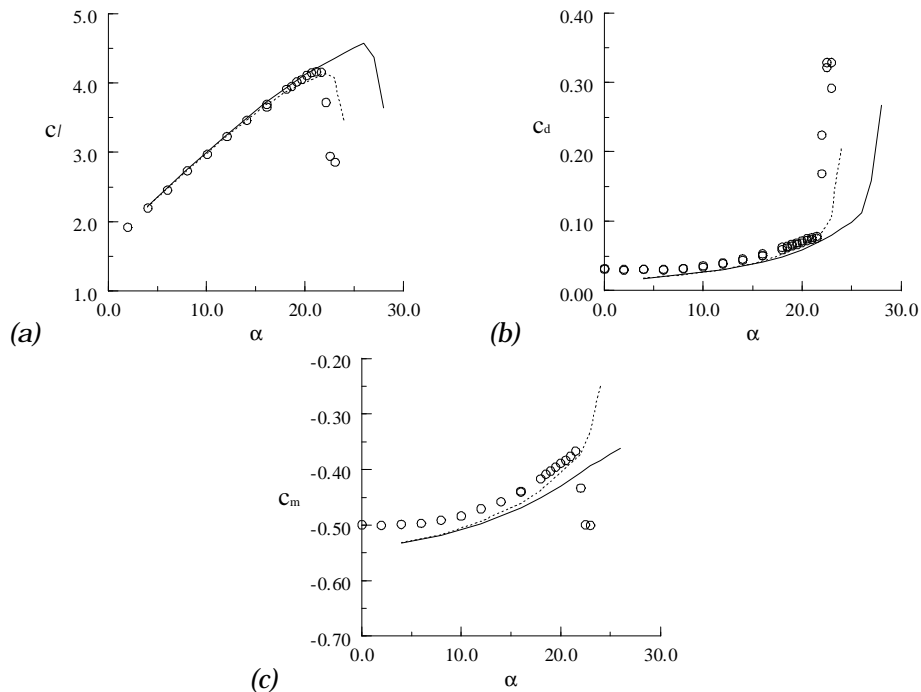


Figure 14. Comparison of calculated (lines) and measured (symbols) (a) lift, (b) drag, and (c) moment coefficients. Continuous lines denote original wake turbulence model and dotted lines modified wake turbulence model.

Also, Figure 14 shows that, while agreement is excellent up to  $\alpha = 20^\circ$ , the original turbulence model in the wake does not allow capturing the stall. However, when the constant  $l_w$  in Eq. (14) is increased to 100, as shown in dotted lines in Figure 14, the stall behavior is captured accurately. Figure 15, which presents the variation of displacement thickness along the chord for each element at  $\alpha = 20^\circ$ , illustrates the growth of the displacement thickness in the main element wake induced by the presence of the flap. Work is in progress to incorporate a turbulent wake formulation similar to that used on the body to improve current predictions. More importantly, these results demonstrate the need for accurately modeling the turbulent shear layers developing in wakes with adverse pressure gradient in order to calculate the stall of multi-element airfoils.

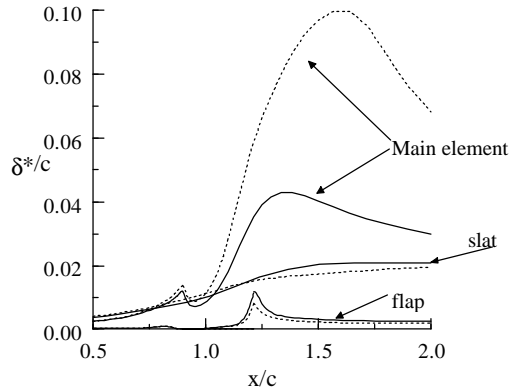


Figure 15. Displacement thickness distribution at  $\alpha = 20^\circ$  for the three-element airfoil. Continuous lines denote calculations performed with the original wake turbulence model and dotted lines with the modified turbulence model.

## Results and Discussion: Three-dimensional Flows

### Single-element Wing

The calculation method is applied in this section to a wing tested by Lovell (1977) at a mean aerodynamic chord Reynolds number of  $1.35 \times 10^6$  with various high lift devices. This wing has an aspect ratio of 8.35, a quarter chord sweep angle of  $28^\circ$ , and no twist. Results obtained for the wing with slat and flap retracted are presented in this section.

Calculations were made by using the panel method, the inverse boundary layer method, and the stability/transition method previously described. At higher angles of attack, the boundary layer calculations showed some numerical oscillations in the wake. For this reason, the calculations were repeated, this time by solving the quasi-three-dimensional boundary layer equations. Calculated lift and drag coefficients for the single-element wing are presented and compared with experimental data in Figure 16. Inviscid results are also presented to show how the introduction of viscous effects allows obtaining results in excellent agreement with data up to an angle of  $10^\circ$ . Beyond this angle of attack, some discrepancies exist and the stall of the wing is slightly over-predicted. This may be due to the use of the quasi-three-dimensional boundary-layer equations. The discrepancy may, however, be due to the accuracy of the turbulence model for three-dimensional flows. These areas are currently under investigation.

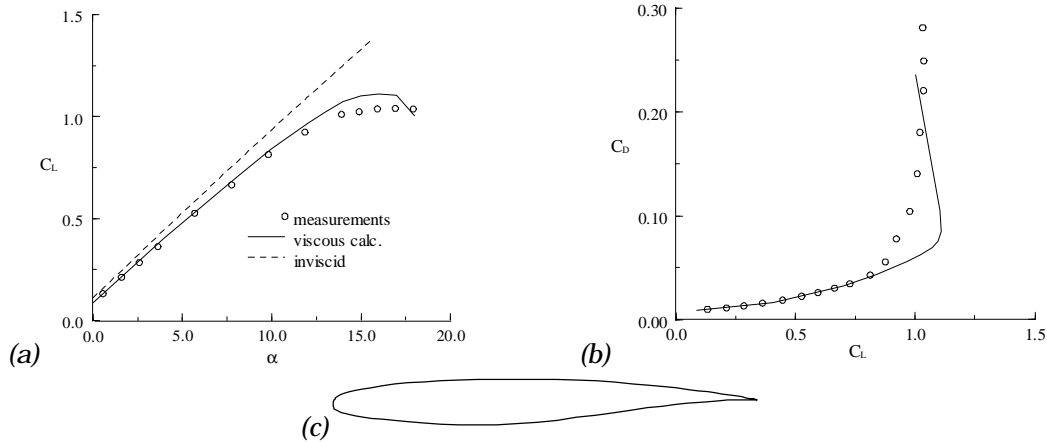


Figure 16. Comparison of measured and computed (a) lift and (b) drag coefficients for the RAE wing with (c) slat and flap retracted.

### Multi-element Wings

Results for the wing of the previous section with slat and flap deployed are presented here. Due to numerical oscillations encountered in the tip region at higher angles of attack, the calculations in this case were performed using the strip theory boundary-layer approximation. For the single element wing, however, no major differences were observed between results obtained with strip theory and those obtained using the quasi-three-dimensional boundary layer approach.

Figure 17 shows a typical paneling of the wing used for the inviscid method. Figure 18 shows a comparison of measured and calculated lift and drag coefficients for the wing with the flap deployed at  $25^\circ$  and the slat either retracted or deployed at  $25^\circ$ . Again, the influence of the viscous effects on the solution is clearly observed and well predicted. In general, results at moderate angles of incidence are not quite as good as for the single element wing. This discrepancy may be due to the merging of the main element wake with the boundary layer developing on the flap upper surface which was not accounted for in the present method. Also, when the slat is deployed, results (dotted lines) at low angles of incidence do not agree as well with experimental data (filled circles). As depicted in Figure 18c, in order to retract the slat and the flap, the slat and main element lower surfaces present discontinuities. These were removed in the calculations by placing fairings, and, therefore, the recirculating flow region in the slat cove—larger at low angles of incidence—was not modeled. Cove calculations, however, could be incorporated by extending the method of Cebeci, Besnard, and Chen (1996) to three-dimensional flows. Finally, other high lift configurations not reported here were tested with the method and, except for the configuration with the slat at  $25^\circ$  and the flap at  $10^\circ$ , stall generally is not well captured. As for the single element wing, the turbulence modeling and the approximations made in the boundary layer solutions may be at the sources of the discrepancies.

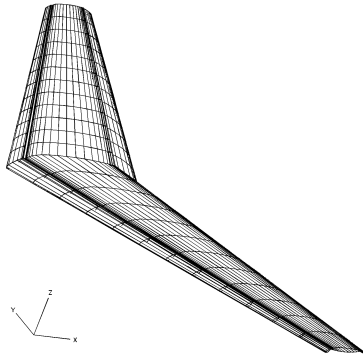


Figure 17. Multi-element wing paneling with slat and flap deployed at 25° -wakes omitted.

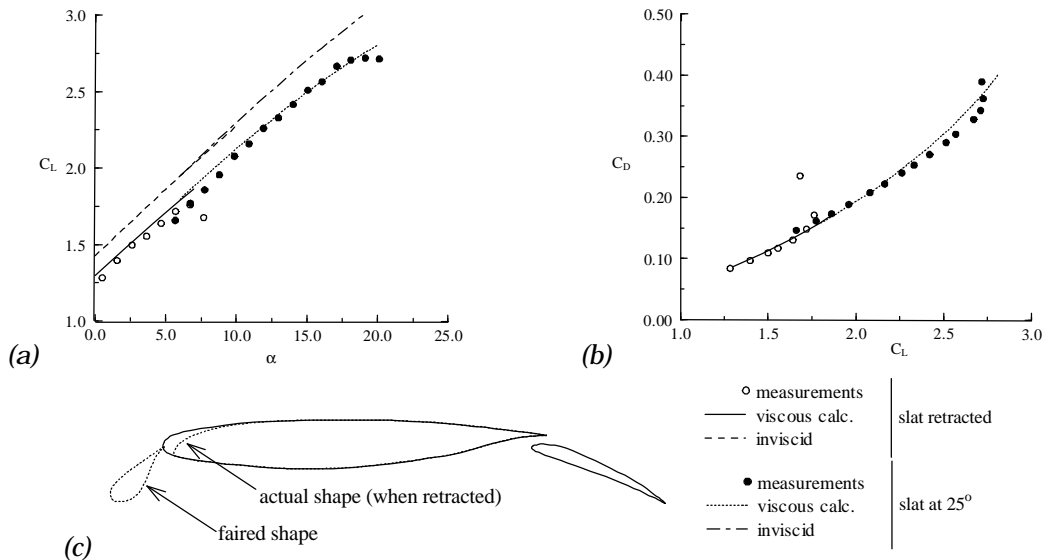


Figure 18. Comparison of measured and computed (a) lift and (b) drag coefficients for the RAE wing with (c) the slat retracted or at 25° and the flap at 25°.

### Concluding Remarks

An interactive boundary-layer method with an improved Cebeci-Smith eddy viscosity formulation is used to calculate the aerodynamic performance characteristics of high lift systems. Results for two-dimensional flows show good agreement with measurements for a variety of multi-element airfoils comprising slats, main element and flaps. In general, the predictions are excellent for relatively low angles of attack and very satisfactory up to stall. The study shows that the onset of transition location plays a significant role in predicting drag and that its calculation must be a part of the computational method. The study also shows that for some flows merging of shear layers takes place and, since the present method does not account for this merging, calculated results, while satisfactory, show some discrepancy with measurements.

The stall prediction is satisfactory for most cases. However, when the pressure peak on the main element reaches values close to or greater than the critical pressure coefficient, a truly compressible inviscid method, such as a full potential or Euler method, should be employed. Also, the need for accurate turbulence models for wake flows is stressed in order to compute stall accurately.

For three-dimensional flows, unfortunately, the available experimental data is limited. The calculations for one wing with several high lift devices deployed show good

agreement with data but the prediction of the stall angle is not as satisfactory as in two-dimensional flows. In addition, the numerical method and the turbulence model need some improvement.

### References

Abbott, I.H., and Von Doenhoff, A.E. (1959). *Theory of Wing Sections*, Dover Publications, Inc., NY, 1959.

Van den Berg, B., and Oskam, B. (1979). "Boundary Layer Measurements on a Two-Dimensional Wing with Flap and a Comparison with Calculations," *AGARD CP-271*, Sept. 1979.

Cebeci, T. (1998). *An Engineering Approach to the Calculation of Aerodynamic Flows*, to be published.

Cebeci, T., Besnard, E., and Chen, H.H. (1996). "Calculation of Multi-element Airfoil Flows, Including Flap Wells," AIAA Paper No. 96-0056, Jan. 1996.

Cebeci, T., and Chang, K.C. (1996). "An Improved Cebeci-Smith Turbulence Model for Boundary-Layer and Navier-Stokes Methods," *Proceedings of the 20<sup>th</sup> ICAS/AIAA Aircraft System Conference*, Sept. 1996.

Cebeci, T., and Smith, A.M.O. (1974). *Analysis of Turbulent Boundary Layers*, Academic Press, 1974.

Cousteix, J., and Pailhas, G. (1979). "Étude Exploratoire d'un Processus de Transition Laminaire-Turbulent au Voisinage du Décollement d'une Couche Limite Laminaire," T.P. No. 1979-86. Also *La Recherche Aérospatiale*, No. 1979-3, pp. 213-218.

Lovell, D.A. (1977). "A Wind-Tunnel Investigation of the Effects of Flap Span and Deflection Angle, Wing Planform and a Body on the High-Lift Performance of a 28° Swept Wing," R.A.E., C.P. No. 1372, Farnborough, U.K.1977.

McGhee, R.J., Jones, G.S., and Jouty, R., (1988). "Performance Characteristics from Wind Tunnel Tests of a Low Reynolds Number Airfoil," AIAA Paper No. 88-0607, Jan. 1988.

Moir, I.R.M. (1994). "Measurements on a two-dimensional Aerofoil with High-Lift Devices," *AGARD-AR-303*, Test Case A-2, 1994.

Nield, N.B., (1995). "An Overview of the 777 High Lift Aerodynamic Design," *Proceedings of High Lift and Separation Control Conference*, Royal Aeronautical Society, March 1995.

Omar, E., Zierten, T., and Mahal, A. (1977). "Two-Dimensional Wind Tunnel Tests of a NASA Supercritical Airfoil with Various High Lift Systems," *NASA CR-2215*, 1977.

Verhoff, A., Chen, H.H., and Cebeci, T. (1996). "An Accurate and Efficient Interactive Boundary Layer Method for Analysis and Design of Airfoils," AIAA Paper No. 96-0328, 1996.